Role of *Toxoplasma gondii* Myosin A in Powering Parasite Gliding and Host Cell Invasion

Markus Meissner,[1] Dirk Schlüter,[2] Dominique Soldati[1]*

Obligate intracellular apicomplexan parasites rely on gliding motion powered by their actomyosin system to disperse throughout tissues and to penetrate host cells. *Toxoplasma gondii* myosin A has been implicated in this process, but direct proof has been lacking. We designed a genetic screen to generate a tetracycline-inducible transactivator system in *T. gondii*. The *MyoA* gene was disrupted in the presence of a second regulatable copy of *MyoA*. Conditional removal of this myosin caused severe impairment in host cell invasion and parasite spreading in cultured cells, and unambiguously established the pathogenic function of this motor in an animal model.

Among the many vital functions of an obligate intracellular parasite, host cell invasion is a prerequisite for survival and replication, and this process is dependent on the ability of *T. gondii* to glide (*1*). Gliding motility requires an intact actin cytoskeleton (*2*) and is likely to be powered by the small unconventional myosin A (TgMyoA or simply MyoA) (*3*, *4*). This motor is found right beneath the plasma membrane and exhibits the transient adenosine triphosphatase kinetics and biophysical properties necessary to generate fast movement (*5*). Additionally, this small myosin of the class XIV and its associated myosin light chain are extremely conserved throughout the *Apicomplexa* (*5*). To date, all attempts to disrupt the *MyoA* gene have failed. Thus, we tried to establish a system for conditional gene knockout to study this gene in vivo.

An inducible system based on the tetracycline repressor (TetR) has been reported for the control of gene expression in several protozoan parasites and is best optimized in *Trypanosoma brucei* (*6*). Indeed, existence of trans-splicing in *kinetoplastida* offers a unique opportunity to combine the tetracycline-dependent repression with the T7 polymerase transcription. However, the more potent and broadly used tet-transactivator system (tTA composed of TetR-VP16 fusion) (*7*) has not been used in parasites. The TetR can control gene expression in *T. gondii* (*8*) but the tTA system is totally inactive. The repression system is suitable for expression of toxic genes and of dominant-negative mutants but is inappropriate for the generation of conditional knockouts. Here, random integration was used to trap a transactivating domain functioning as tet-dependent transactivator when fused to TetR. The plasmid used for random insertion contained the dehydrofolate reductase–thymidylate synthase gene (*Tg-DHFR-TS*), conferring pyrimethamine (pyr) resistance and exhibiting a very high frequency of integration (10^{-2}). This vector was linearized before transfection, immediately downstream of a TetR expression cassette that contained no stop codon and no 3′ UTR sequences. The recipient parasite line used for the random insertion screening was engineered to express both *HXGPRT* and LacZ genes under the control of a tet-dependent transactivator [Fig. 1A (*9*)]. In the absence of a functional tet-transactivator, the promoter was silent; consequently, HXGPRT was not expressed, and the recipient strain was sensitive to mycophenolic acid (MPA). After random insertion, positive clones were selected for their ability to express LacZ and HXGPRT in an anhydrotetracycline (ATc)-dependent fashion. One of the clones, named TATi-1 (trans-activator trap identified), showed tightly inducible LacZ expression (Fig. 1B). The corresponding transactivator was isolated by reverse transcription–polymerase chain reaction (RT-PCR) amplification of the TetR 3′ end extension. In contrast to the VP16-activating domain, the 26–amino acid COOH-terminal extension of TATi-1 (Fig. 1C) was not acidic but hydrophobic, and showed no homologies to transcription factors or known proteins. A cell line expressing TATi-1 was generated to establish a convenient inducible system, and TATi-1 function was assessed by transient transfection with p7TetOLacZ, resulting in strong ATc-dependent LacZ expression (Fig. 1D). In contrast, transfection of this reporter vector in wild-type parasites or those expressing synthetic $tTA2^s$ (*8*) showed no significant β-galactosidase activity.

To generate a conditional knockout of *MyoA*, a second copy of the gene controlled by the tet-inducible promoter (*MyoAi*) was integrated at random into the genome of the TATi-1–expressing cell line (*MyoAe*, containing the endogenous copy). The resulting

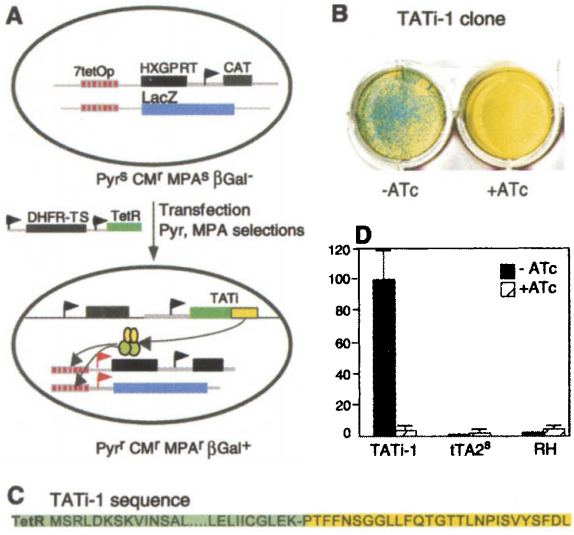

Fig. 1. Trapping of a functional transactivator by random insertion in *T. gondii* genome. (**A**) Scheme of the trap strategy. A recipient strain for the screen was generated by stable integration of two plasmids expressing HXGPRT and LacZ under the control of a tet-transactivator responsive promoter (*9*), using the chloramphenicol acetyltransferase gene (*CAT*) as selectable marker. A linear DNA vector expressing *DHFRTS* that conferred resistance to pyr and encoded the TetR without a stop codon was integrated at random into the genome of the recipient strain. The transformants were selected with MPA for HXGPRT expression and then screened for LacZ expression. In clones fulfilling both criteria, the tetR vector integrated into a locus that had created a functional transactivator (TetR fusion with a transactivating domain). (**B**) The parasite clone expressing TATi-1–regulated LacZ expression in ATc-dependent manner as determined by X-Gal staining (*8*). (**C**) Amino acid sequence of the transactivating domain of TATi-1 (in yellow) fused at the COOH-terminus of TetR (in green). Abbreviations for the amino acid residues: A, Ala; C, Cys; D, Asp; E, Glu; F, Phe; G, Gly; I, Ile; K, Lys; L, Leu; M, Met; N, Asn; P, Pro; Q, Gln; R, Arg; S. Ser; T. Thr; V, Val; and Y, Tyr. (**D**) Transient transfection of p7TetOS1LacZ into RH or in parasites expressing TATi-1 or the synthetic tetracycline-controlled transactivator $tTA2^s$. Cells were grown for 48 hours in presence or absence of ATc before quantification of LacZ expression, as described (*8*). The vertical axis reports the percentage of β-galactosidase activity. TATi-1–driven LacZ activity, in absence of ATc, was fixed to 100%.

[1]Department of Biological Sciences, Imperial College of Science, Technology and Medicine, Imperial College Road, London SW7 2AZ, UK. [2]Institut für Med. Mikrobiologie und Hygiene, Universitätsklinikum Mannheim, Theodor-Kutzer-Ufer 1-3, 68167 Mannheim, Germany.

*To whom correspondence should be addressed. E-mail: d.soldati@ic.ac.uk

cell line exhibited both the endogenous and the inducible copy and was named *MyoAe/MyoAi*. Modulation of transgene expression by ATc treatment was monitored by immunofluorescence (Fig. 2A) and by Western blot (Fig. 2B and Table 1), which revealed that the robustness of TATi-1 induction reached 60% of the endogenous level of MyoA expression. The presence of *MyoAi* allowed us to ablate the endogenous *MyoAe* gene by double homologous recombination. Two independent stable clones, named *Δmyoa1/MyoAi* and *Δmyoa2/MyoAi*, lacked the *MyoAe* gene (Fig. 2C). The absence of MyoAe, which migrates slightly faster than the epitope-tagged inducible MyoAi (Fig. 2D), was also confirmed, as was repression of MyoAi expression (Fig. 2E and Table 1).

The role of MyoA in parasite motion was determined by scoring the percentage of parasites gliding on coated glass slides with the use of time-lapse microscopy (*9*). In optimal conditions, about 20% of freshly released parasites (*MyoAe*) glided, and they showed all three forms of motility (circular gliding, upright twirling, and helical gliding) (*10*). Under these conditions, less than 10% of *Δmyoa1/MyoAi* parasites were motile, performing a reduced number of circles or incomplete circles at a lower speed than *MyoAe* parasites (*9*) (Movies S1 to S5). In sharp contrast, *Δmyoa1/MyoAi* parasites depleted in MyoAi were totally unable to glide (Table 1).

The consequence of impairment in gliding motility was examined for cell-to-cell spreading, a more complex physiological process, which is easily visualized by plaque assay. Seven days after inoculation of fibroblast monolayers, clonal growth of individual parasites generated plaques of lysis. Depletion of MyoAi in *Δmyoa1/MyoAi* completely inhibited the formation of large plaques. Expression of MyoAi led to plaques slightly smaller than the ones generated by *MyoAe* parasites (Fig. 3A).

To establish whether *Δmyoa1/MyoAi* depleted in MyoAi were impaired in their ability to invade host cells, we treated intracellular parasites for 48 to 72 hours with or without ATc and analyzed them by invasion assays. The *MyoAe/MyoAi* parasites showed no alteration of invasion upon ATc treatment, but the efficiency of invasion by *Δmyoa1/MyoAi* was vastly reduced, with less than 20% of the parasites capable of infection compared with untreated parasites (Fig. 3B). All of the parasites that managed to invade host cells were analyzed 24 hours later for intracellular growth by counting the number of parasites per vacuole. Because of the lack of synchronization, the vacuoles contained 2, 4, 8, or 16 parasites. The distribution of the number of parasites per vacuole did not significantly differ for *Δmyoa1/MyoAi* and *MyoAe/MyoAi*. Thus, neither the depletion of MyoAi nor ATc treatment affected the rate of intracellular growth (Fig. 3C).

T. gondii uses similar molecular mechanisms for egress and invasion (*11–13*). After lysis of the host cell and the parasitophorous vacuole, motile parasites rapidly spread over neighboring cells, relying on their gliding motion. Increases in intracellular calcium with the use of the calcium ionophore A23187 stimulate microneme secretion and induce intracellular parasite egress (*11*). We monitored the time-dependent A23187-stimulated egress on parasites cultivated for 36 hours with or without ATc (Fig. 3D). *Δmyoa1/MyoAi* parasites expressing MyoAi were motile, but disseminated slightly less efficiently than wild-type parasites (Fig. 3E). In contrast, *Δmyoa1/MyoAi* parasites depleted in MyoAi were markedly hampered in spreading from the lysed vacuole. The egress assay indirectly monitors the ability of parasites to glide on host cells and allows the examination of fit parasites in the absence of any manipulation. Time-lapse microscopy of parasites stimulated to egress revealed a slight decrease in the speed of spreading of *Δmyoa1/MyoAi* compared with *MyoAe* parasites. When depleted in MyoAi, *Δmyoa1/MyoAi* parasites were unable to leave the host cells and showed no significant movement (*9*) (Movies S6 to S8).

The apical organelles, called micronemes, release transmembrane adhesin complexes, which are necessary for parasite gliding and host cell invasion (*14–15*). An impairment of microneme secretion would presumably lead to phenotypic consequences as described above. To exclude involvement of MyoA in

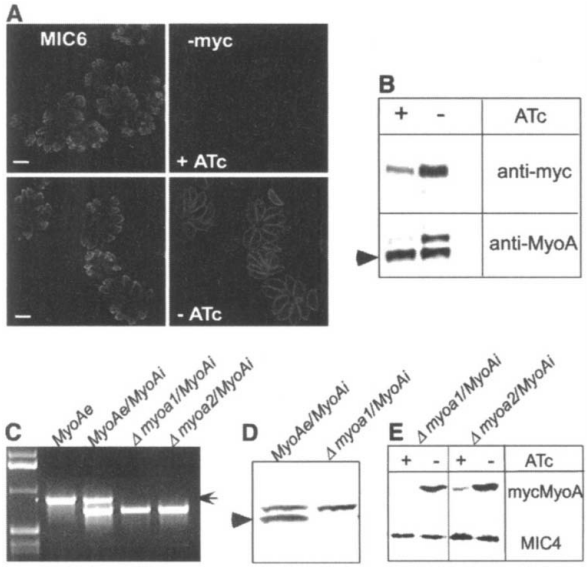

Fig. 2. A conditional knockout of the *MyoA* gene. (**A**) Regulation of MyoAi expression by ATc. *MyoAe/MyoAi* parasites grown with or without ATc for 48 hours were fixed and stained with antibodies to Myc (right panels) and antibodies to MIC6 (left panels) as control. Micrographs were taken under identical exposure conditions by confocal microscopy. Scale bar, 5 μm. (**B**) Immunoblot of MyoAi expression in *MyoAe/MyoAi* parasites was revealed with an antibody against Myc, and both endogenous (arrowhead) and inducible (upper band) MyoA proteins were detected with polyclonal antibodies to the tail of MyoA. As internal standard, lysates were probed with an antibody against MIC6. (**C**) Detection of endogenous and inducible copies of *MyoA* by genomic PCR on *MyoAe*, *MyoAe/MyoAi*, *Δmyoa1/MyoAi*, and *Δmyoa2/MyoAi* parasites. Sequence-specific primers amplified endogenous (in intron) and inducible (in 5′ UTR) genomic fragments. An arrow indicates the fragment corresponding to the endogenous copy. (**D**) Western blot analysis of *Δmyoa1/MyoAi* with antibodies against MyoA showing that this clone lacked endogenous MyoA (arrowhead). (**E**) Repression of MyoAi expression in *Δmyoa1/MyoAi* and *Δmyoa2/MyoAi* parasites 48 hours after growth with or without ATc. MIC4 was used as control for equal loading.

Table 1. The percentage of freshly released parasites showing gliding motion has been determined from four independent experiments (numbers in parentheses denote standard variation). *Δmyoa1/MyoAi* parasites expressing MyoAi were predominantly twirling and showed reduced circular and helical gliding. The circles were frequently incomplete and performed at a reduced speed compared with wild-type parasites. The other values listed in this table are summarizing the results presented in Figs. 2, 3, and 4 (ns, data not shown). The column MyoAe/MyoAi reports the quantification of MyoAe and MyoAi protein determined by scanning the immunoblots (Fig. 2).

Strain	ATc	MyoAe/MyoAi	Gliding	Invasion	Egress	Plaques	Virulence in mice (% death)
MyoAe (wt)	–	1.0/0	22% (6)	ns	92%	large	100
MyoAe (wt)	+	1.0/0	16% (4)	ns	88%	large	100
MyoAe/MyoAi	–	0.9/0.6	ns	100%	ns	large	100
MyoAe/MyoAi	+	1.0/0.1	ns	107% (12)	ns	large	100
Δmyoa1/MyoAi	–	0/0.6	8% (2)	100%	75%	medium	100
Δmyoa1/MyoAi	+	0/0.05	0%	16% (4)	18%	very small	0

microneme exocytosis, we examined the ability of Δ*myoa1/MyoAi* parasites to discharge their content upon ethanol stimulation (*16*). Detection of secretion of the microneme protein 4 (MIC4) is a convenient diagnostic of exocytosis, because its secretion is accompanied by two post-exocytic processing events leading to the release of a 50-kD product (*17*). There was no significant reduction in MIC4 discharge from Δ*myoa1/MyoAi* after MyoAi depletion (Fig. 3F). Thus, the impairment of cell-to-cell spreading observed in the absence of MyoA was linked to the inability of the parasites to glide and not to a defect in organelle exocytosis.

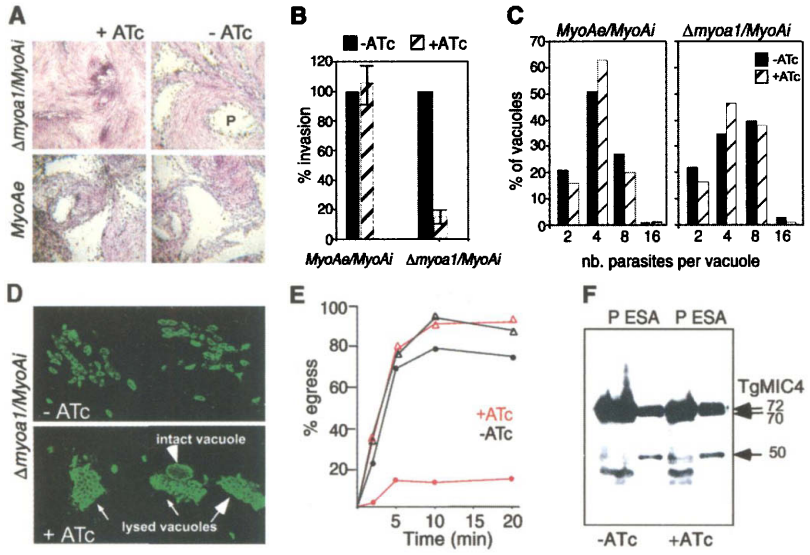

Fig. 3. Phenotypic consequences of MyoA depletion for parasite propagation in culture. (**A**) Plaque assays for *MyoAe* and Δ*myoa1/MyoAi* parasites grown on human foreskin fibroblasts, in the presence or absence of ATc for 7 days before fixation and staining with Giemsa. (**B**) Invasion assays of Δ*myoa1/MyoAi* compared with *MyoAe/MyoAi* parasites, from three independent experiments (*9*). The number of vacuoles represents a percentage of 100% (which reflects successful invasion) in the absence of ATc for *MyoAe* and Δ*myoa1/MyoAi*, respectively. (**C**) The rate of intracellular growth was monitored 24 hours after invasion by counting the number of parasites per vacuole. Three independent experiments (one representative shown here) indicated no impairment in intracellular growth between *MyoAe/MyoAi* and Δ*myoa1/MyoAi*. (**D**) Egress assays of Δ*myoa1/MyoAi* parasites upon A23187 treatment, followed by fixation, staining with an antibody against SAG1, and confocal microscopy (*9*). (**E**) Time course of egress monitored after A23187 treatment. The triangles correspond to wild-type *MyoAe* and the circles correspond to Δ*myoa1/MyoAi* parasites. (**F**) Microneme secretion assay upon ethanol stimulation of Δ*myoa1/MyoAi* parasites. Western blot analysis of MIC4 in parasite pellets (P) and in excretory secretory antigens (ESA) monitored the parasites' ability to secrete. MIC4 is processed after exocytosis into several smaller products. The 70- and 50-kD forms are detectable with antibody against MIC4 (*17*).

To investigate the role of MyoA during animal infection and to validate the inducible system in vivo, we infected groups of mice with Δ*myoa1/MyoAi* parasites and supplemented the drinking water for some groups with ATc. The strain of *T. gondii* used in this study is RH, a type I strain, which typically kills mice with the lethal dose (LD) of a single infectious parasite (*18*). To assess the virulence of Δ*myoa1/MyoAi*, 150 parasites were inoculated intraperitoneally (i.p.) (*9*). Eight days after infection, all of the mice infected with Δ*myoa1/MyoAi* (Fig. 4A) had died. In contrast, when the drinking water was supplemented with ATc, 100% survival of the mice was observed 11 days after infection. At this time ATc was withdrawn. At day 17 after infection, these animals had developed *T. gondii* T and B cell–specific responses, as determined by an interferon-γ specific ELISPOT [Fig. 4B (*9*)] and immunoblot. To determine whether these mice were protected against a subsequent challenge infection, they were inoculated i.p. with 150 wild-type parasites on day 17 after infection. All challenged mice survived, which indicates that Δ*myoa1/MyoAi* had induced a protective immunity (Fig. 4A).

The transactivator described here was instrumental in the generation of a conditional knockout for a virulence gene in an apicomplexan. This system establishes that the small class XIV myosin A powers gliding motility. Moreover, the depletion of this myosin markedly impaired the ability of parasites to invade and egress, linking parasite motion to invasion (Table 1). The exact mechanism by which this unconventional motor contributes to gliding motility and, more specifically, how it redistributes transmembrane adhesins toward the posterior pole of the parasite, remains to be elucidated. Depletion of MyoA in infected mice demonstrates that this gene is a virulence factor, and it validates that this inducible system can be used for the modulation of parasite gene expression in animal studies. TATi-1 represents a *T. gondii*–specific transactivator, and it remains to be seen if this factor functions in other apicomplexans, particularly in the closely related parasite *Plasmodium falciparum*, potentially allowing development of an inducible system for malarial parasites.

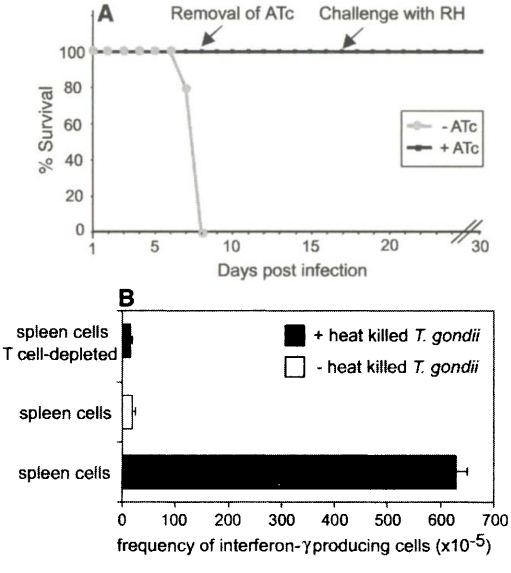

Fig. 4. Parasites depleted in MyoA are avirulent in mice and confer protection against a new challenge. (**A**) *MyoAe* or Δ*myoa1/MyoAi* tachyzoites were injected i.p. into BALB/c mice and monitored for more than 30 days. Groups of mice were given drinking water with or without ATc (0.2 mg/ml). After 11 days, only the group of 10 mice infected with Δ*myoa1/MyoAi* and treated with ATc survived. At day 17 after infection, these animals were challenged with 150 parasites of the RH strain, and they survived the infection. (**B**) Induction of *T. gondii*–specific T cells after infection with Δ*myoa1/MyoAi*. At day 17 after infection, spleen cells were isolated from Δ*myoa1/MyoAi*-infected mice treated with ATc, and the frequency of *T. gondii*–specific T cells was determined by interferon-γ ELISPOT. In uninfected mice, spleen cells did not produce interferon-γ after stimulation with heat-killed *T. gondii*. The mean of triplicates ± SD is shown.

References and Notes

1. L. D. Sibley, S. Hakansson, V. B. Carruthers, *Curr. Biol.* **8**, 12 (1998).
2. J. M. Dobrowolski, L. D. Sibley, *Cell* **84**, 933 (1996).
3. M. B. Heintzelman, J. D. Schwartzman, *J. Mol. Biol.* **271**, 139 (1997).
4. C. Hettmann *et al.*, *Mol. Biol. Cell* **11**, 1385 (2000).
5. G. Herm-Götz *et al.*, *EMBO J.* **21**, 2149 (2002).

6. E. Wirtz, S. Leal, C. Ochatt, G. A. Cross, *Mol. Biochem. Parasitol.* **99**, 89 (1999).
7. M. Gossen, H. Bujard, *Proc. Natl. Acad. Sci. U.S.A.* **89**, 5547 (1992).
8. M. Meissner *et al.*, *Nucleic Acids Res.* **29**, e115 (2001).
9. Materials and methods are available as supporting material on *Science* Online.
10. S. Hakansson, H. Morisaki, J. Heuser, L. D. Sibley, *Mol. Biol. Cell* **10**, 3539 (1999).
11. M. Black, G. Arrizabalaga, J. C. Boothroyd, *Mol. Cell. Biol.* **20**, 9399 (2000).
12. R. Moudy, T. J. Manning, C. J. Beckers, *J. Biol. Chem.* **276**, 41492 (2001).
13. E. F. Hoff, V. B. Carruthers, *Trends Parasitol.* **18**, 251 (2002).
14. A. A. Sultan *et al.*, *Cell* **90**, 511 (1997).
15. V. B. Carruthers, O. K. Giddings, L. D. Sibley, *Cell Microbiol.* **1**, 225 (1999).
16. V. B. Carruthers, S. N. Moreno, L. D. Sibley, *Biochem. J.* **342**, 379 (1999).
17. S. Brecht *et al.*, *J. Biol. Chem.* **276**, 4119 (2000).
18. E. R. Pfefferkorn, L. C. Pfefferkorn, *Exp. Parasitol.* **39**, 365 (1976).
19. Supported by Deutsche Forschungsgemeinschaft grant SO366/1-3. We are grateful to L. Y. Kwok, K. Schönig, and A. Herm-Götz for their assistance, and S. Brecht and C. Hettmann for their contributions to the early phase of the project. Special thanks to T. Soldati for his assistance with the microscopy and considerable input in the project, H. Bujard for helpful discussions, and R. Sinden for critical reading of the manuscript.

Supporting Online Material
www.sciencemag.org/cgi/content/full/298/5594/837/DC1
Materials and Methods
Movies S1 to S8

31 May 2002; accepted 4 September 2002

Oscillatory Expression of the bHLH Factor Hes1 Regulated by a Negative Feedback Loop

Hiromi Hirata,[1] Shigeki Yoshiura,[1] Toshiyuki Ohtsuka,[1]* Yasumasa Bessho,[1] Takahiro Harada,[2] Kenichi Yoshikawa,[2] Ryoichiro Kageyama[1]†

Transcription of messenger RNAs (mRNAs) for Notch signaling molecules oscillates with 2-hour cycles, and this oscillation is important for coordinated somite segmentation. However, the molecular mechanism of such oscillation remains to be determined. Here, we show that serum treatment of cultured cells induces cyclic expression of both mRNA and protein of the Notch effector Hes1, a basic helix-loop-helix (bHLH) factor, with 2-hour periodicity. Cycling is cell-autonomous and depends on negative autoregulation of *hes1* transcription and ubiquitin-proteasome–mediated degradation of Hes1 protein. Because Hes1 oscillation can be seen in many cell types, this clock may regulate timing in many biological systems.

Although circadian clocks have been well characterized (*1*), other molecular clocks that regulate many biological processes, such as embryogenesis, are not known. It has been shown that mRNAs for Notch signaling molecules such as the bHLH factor Hes1 oscillate with 2-hour cycles during somite segmentation, which occurs every 2 hours (*2–9*). However, the molecular mechanism of such oscillation remains to be determined.

We have found that *hes1* transcription is induced in stationary cultured cells upon stimulation by serum (*10*). However, induced levels of expression were variable, depending on when measurements were taken. We therefore examined the time course of *hes1* mRNA induction in detail. A single serum treatment induces 2-hour cycle oscillation of *hes1* mRNA in a variety of cultured cells, such as myoblasts (C2C12) (Fig. 1A), fibroblasts (C3H10T1/2), neuroblastoma cells (PC12), and teratocarcinoma cells (F9) (*10, 11*). This oscillation continues for 6 to 12 hours, corresponding to three to six cycles (Fig. 1A).

Hes1 protein also oscillates in a 2-hour cycle after a single serum treatment (Fig. 1B). Protein oscillation is delayed by ~15 min relative to the mRNA oscillation (Fig. 1C). This time delay may reflect the time required for protein degradation. The *hes1* mRNA and Hes1 protein oscillations in cultured cells are not dependent on the inductive stimulus: They are also induced by exposure to cells expressing Delta (fig. S1), which is known to up-regulate Hes1 expression via Notch signaling (*12, 13*). *hes1* oscillation is observed in cells treated with Ara-C, an inhibitor of DNA replication, suggesting that cell cycle progression is not relevant to Hes1 oscillation (*10*).

We next examined the half-lives of *hes1* mRNA and Hes1 protein (*11*). The half-life of *hes1* mRNA was found to be 24.1 ± 1.7 min (fig. S2A) whereas that of Hes1 protein was about 22.3 ± 3.1 min (fig. S2B). The half-life of Hes1 protein is even shorter than that of c-Fos protein (~2 hours), which is known to disappear rapidly after immediate-early induction (*14*). The short half-lives for *hes1* mRNA and Hes1 protein may enable such a 2-hour cycle oscillation. The instability of *hes1* mRNA could be regulated by the 3′-untranslated region, as revealed for other *hes1*-related mRNAs (*15*).

To identify proteases responsible for Hes1 protein degradation, we tested various protease inhibitors for their ability to stabilize Hes1 protein. Application of proteasome inhibitors [lactacystin, MG132, and *N*-acetyl-Leu-Leu-norleucinal (ALLN)] (*16*) stabilized Hes1 protein and blocked serum-induced Hes1 protein oscillation, whereas other protease inhibitors [leupeptin, phenylmethylsulfonyl fluoride (PMSF), pepstatin A, and *N*-acetyl-Leu-Leu-methioninal (ALLM)] did not (Fig. 2A) (fig. S3); these findings suggest that Hes1 protein is specifically degraded by the ubiquitin-proteasome pathway. To confirm this notion, we expressed Hes1 protein with the hemagglutinin (HA) tag in C3H10T1/2 cells and analyzed it for ubiquitination (*11*). In the presence of the proteasome inhibitor lactacystin, high molecular weight bands (>100 kD) as well as a full-length Hes1 band are detected by antibody to HA (anti-HA) (Fig. 2B, lane 4). Furthermore, these high molecular weight species were found to be highly reactive to anti-ubiquitin, confirming that Hes1 protein is ubiquitinated in cells (Fig. 2B, lane 8).

We next wanted to examine the mechanism for the observed Hes1 oscillation. We previously showed that Hes1, a transcriptional repressor, negatively autoregulates its own expression by directly binding to its own promoter (*17, 18*). Thus, one likely mechanism is that serum-induced Hes1 protein represses *hes1* mRNA synthesis, which leads to rapid loss of Hes1 protein by the ubiquitin-proteasome pathway, and loss of Hes1 protein in turn relieves repression of *hes1* mRNA synthesis. In this model, the oscillation is attributable to negative autoregulation of *hes1* mRNA synthesis by Hes1 protein. If this model is correct, manipulation of the Hes1 protein level should affect *hes1* mRNA oscillation. An alternative model is that Hes1 protein is not an essential component but just an output of a primary clock. In this model, *hes1* mRNA oscillation is regulated by such a clock and not by Hes1 protein. To address this issue, we manipulated the Hes1 protein level and monitored *hes1* mRNA oscillation.

In the presence of the proteasome inhibitor MG132, *hes1* mRNA is transiently induced by a serum treatment, but it remains suppressed persistently thereafter (Fig. 3A).

[1]Institute for Virus Research, Kyoto University, Kyoto 606-8507, Japan. [2]Department of Physics, Graduate School of Science, Kyoto University and CREST, Kyoto 606-8502, Japan.

*Present address: Department of Biological Sciences, Stanford University, Stanford, CA 94305, USA.
†To whom correspondence should be addressed. E-mail: rkageyam@virus.kyoto-u.ac.jp